Ultrasound in Med. & Biol., Vol. 34, No. 9, pp. 1504–1512, 2008
Copyright © 2008 World Federation for Ultrasound in Medicine & Biology
Printed in the USA. All rights reserved
0301-5629/08/$–see front matter

ELSEVIER

doi:10.1016/j.ultrasmedbio.2008.02.001

● *Original Contribution*

ANISOTROPY OF HIGH-FREQUENCY INTEGRATED BACKSCATTER FROM AORTIC VALVE CUSPS

ZAMIR KHAN,*¶ DEREK R. BOUGHNER,*‡§¶ and JAMES C. LACEFIELD*†‡¶

*Biomedical Engineering Graduate Program; †Department of Electrical and Computer Engineering; ‡Department of Medical Biophysics; §Department of Medicine; and ¶Robarts Research Institute, University of Western Ontario, London, Ontario, Canada

(*Received* 15 *October* 2007; *revised* 17 *January* 2008; *in final form* 4 *February* 2008)

Abstract—The biaxial anisotropy of integrated backscatter from aortic valve cusps was characterized *ex vivo* as an initial assessment of the suitability of high-frequency ultrasound for nondestructive evaluation of fiber alignment in tissue-engineered heart valves. Apparent integrated backscatter (AIB) from eight fresh, intact porcine cusps was measured over an 80° range of insonification angles using a 40-MHz ultrasound system. Angular dependence of backscatter was characterized by fitting a sinusoid to plots of AIB *versus* insonification angle for data acquired while rotating the transducer about the cusps in the circumferential and radial directions. Angular variations in backscatter were detected along both directions in individual specimens, although the mean amplitude of the fitted sinusoid was significantly greater for the circumferential data (12.1 ± 2.6 dB) than the radial data (3.5 ± 3.1 dB, $p = 0.002$). The higher angular variation of backscatter in the circumferential direction implies that collagen fibers in the fibrosa layer are the most prominent source of high-frequency scattering from porcine aortic valve cusps. The ability to characterize anisotropic backscattering from individual specimens demonstrates that high-frequency ultrasound can be used for nondestructive evaluation of fiber alignment in heart valve biomaterials. (E-mail: jlacefield@eng.uwo.ca) **© 2008 World Federation for Ultrasound in Medicine & Biology.**

Key Words: **High-frequency ultrasound, Ultrasonic tissue characterization, Integrated backscatter, Anisotropy, Aortic valve.**

INTRODUCTION

The functional durability of the natural aortic valve, which completes 30–40 million cycles annually while withstanding transvalvular pressures of 80 mm Hg (Thubrikar 1995) is remarkable considering the submillimeter thickness of its three cusps. Each cusp is composed of three distinct tissue layers (Fig. 1) whose structural integrity is largely attributed to a complex network of collagen fibers (Vesely and Noseworthy 1992; Christie and Barratt-Boyes 1995). The layer facing the left ventricle, the *ventricularis,* consists of densely packed collagen fibers that are aligned circumferentially and radially in an alternating configuration, as well as radially aligned elastin. The *fibrosa* layer faces the aorta and is composed primarily of circumferentially aligned collagen fibers. The two fibrous layers are joined by the *spongiosa,* a gelatinous lamina composed of loosely arranged collagen, glycosoaminoglycans and water. The ventricularis and fibrosa exhibit structural anisotropy because of their collagen and elastin content, whereas the spongiosa is considered isotropic. In the histology section shown in Fig. 1c, the radially aligned fibers in the ventricularis appear as subtle, approximately horizontal striations, whereas the lack of such striations in the ventricularis implies that the fibers in that layer are predominantly oriented in the circumferential direction. Characterization of this anisotropy has increased scientific understanding of the properties of natural (Doehring et al. 2005) and bioprosthetic (Sacks et al. 1998) valves.

The failure of bioprosthetic aortic valves constructed from porcine or bovine tissues to match the robustness of a native valve motivates investigations of heart-valve tissue engineering. Replication of the complex structure of the native tissue is an accepted requirement (Shi et al. 2006) to achieve long-term durability. A tissue-engineered valve should therefore consist of cusps possessing a layered structure with at least one layer

Address correspondence to: James Lacefield, Department of Electrical and Computer Engineering, University of Western Ontario, 279 Thompson Engineering Building, London, Ontario N6A 5B9, Canada. E-mail: jlacefield@eng.uwo.ca

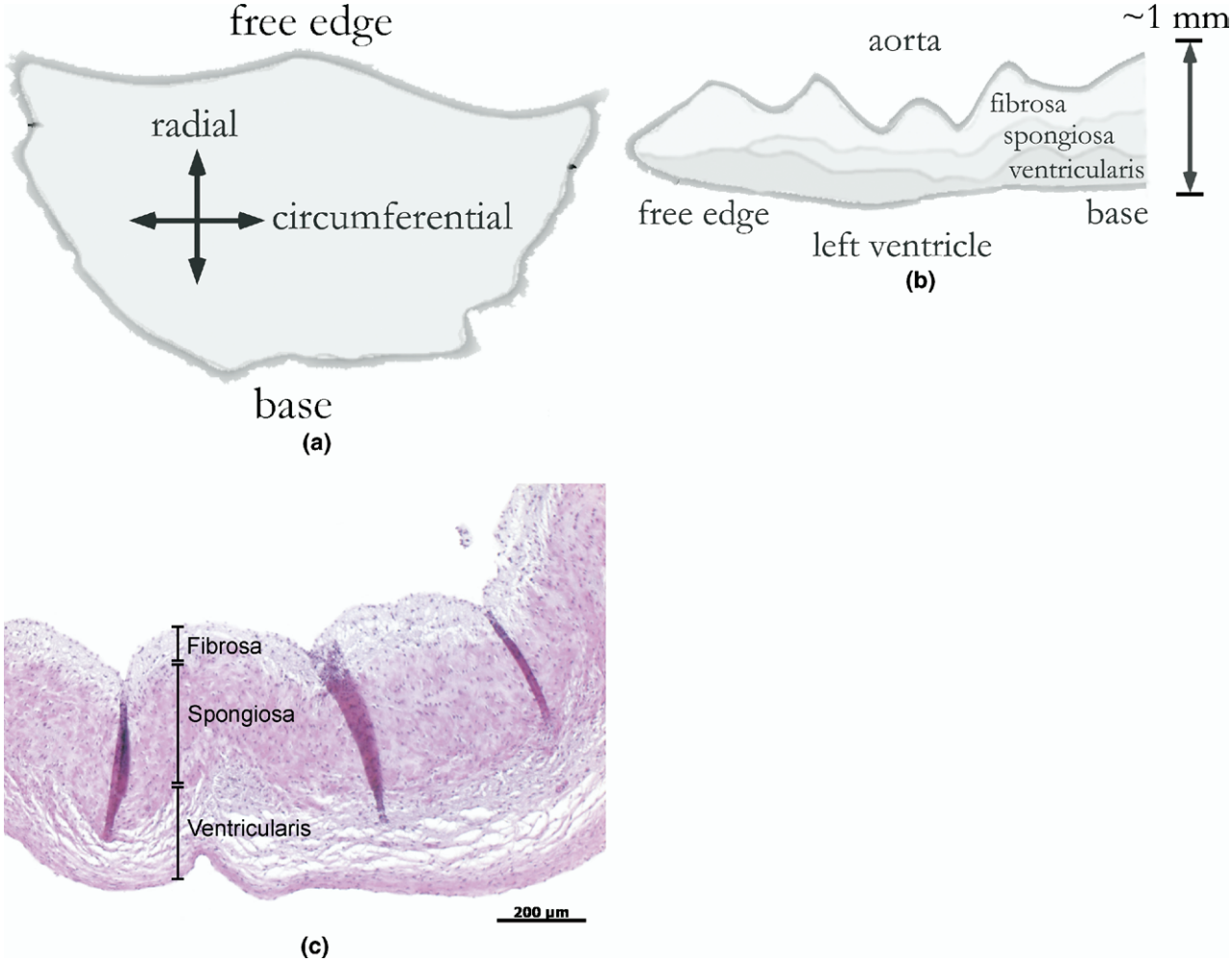

Fig. 1. (a) Schematic illustration of a top view of an aortic valve cusp. (b) Schematic illustration of a radial cross-sectional view of an aortic valve cusp. (c) Hematoxylin and eosin–stained histology slide of a radial slice through a porcine aortic valve cusp specimen.

containing well aligned collagen bundles. The native aortic valve exhibits limited circumferential extensibility as a result of the circumferentially oriented collagen bundles in the fibrosa; yet the valve has good radial extensibility because of the limited collagen fiber alignment in the ventricularis (Vesely 2003). Such a design provides both the flexibility (Vesely and Boughner 1989) and mechanical anisotropy required for proper valve closure (Christie 1992) because the cusps are able to support and effectively distribute the transvalvular pressure applied to their surfaces while simultaneously stretching radially to coapt and seal the orifice during diastole and flexing open to permit ejection of blood during systole. A nondestructive technique for evaluating tissue layering and fiber orientation would therefore be invaluable for assessing a bioengineered material being readied for implantation (Mendelson and Schoen 2006).

Anisotropic microstructure in tissue produces variations in ultrasonic backscatter as a function of the angle of insonification (Mottley and Miller 1988; Rose et al. 1995; Insana 1995). Anisotropic scattering from myocardial tissue has received the greatest attention. Collagen content has a strong influence on backscatter from cardiac tissue (Mimbs et al. 1980; O'Donnell et al. 1981; Lythall et al. 1993), and collagen fibers are hypothesized to be quasi-cylindrical scattering elements responsible for anisotropic backscatter from the myocardium (Rose et al. 1995). Fibrous collagen comprises approximately half of the aortic valve cusp composition by weight (Bashey et al. 1967) and, given the well-defined alignment of collagen in the cusps, it is reasonable to expect ultrasonic backscatter from aortic valve cusps to also exhibit an angular dependence. High-frequency (40 MHz) ultrasound images provide sufficient spatial reso-

lution to delineate the fibrosa, spongiosa and ventricularis layers of aortic valve cusps (Qiu et al. 2006; Khan et al. 2007). Measurements of the angular dependence of high-frequency backscatter therefore offer a promising approach to nondestructive evaluation of fiber orientation in a thin, multilayered tissue such as an aortic valve cusp.

Previous investigations of ultrasonic backscatter from heart valves, conducted at 2–7 MHz, were concerned with assessment of natural and bioprosthetic valve health. Lattanzi et al. (1990) used integrated backscatter index to differentiate normal, fibrotic and calcific mitral valves *in vivo*. Rigolin et al. (2001) used the same backscatter metric, which they termed integrated backscatter amplitude, *in vitro* to distinguish explanted porcine bioprosthetic aortic valves from unused bioprosthetic valves. Both studies associated symptoms of leaflet deterioration with an increase in backscatter intensity from the tissue, but neither study considered the possible anisotropy of backscattering.

In this paper, the anisotropy of apparent integrated backscatter (Hoffmeister et al. 1995) from porcine aortic valve cusps is measured *ex vivo* at 20–47 MHz. This study is the first to characterize the angular dependence of backscattering from aortic valve cusps. Biaxial anisotropy is examined through rotations about two orthogonal axes corresponding to the circumferential and radial directions in the cusps. The results are analyzed using a model of sinusoidal angular dependence of backscatter that assumes quasi-cylindrical scatterers (Mottley and Miller 1988). The parameters estimated using the sinusoidal model demonstrate that the cusps exhibit, on average, a strong angular dependence of backscatter in the circumferential direction and that the measurement technique is capable of detecting anisotropy of backscatter in individual specimens.

MATERIALS AND METHODS

Specimen preparation

Four freshly harvested porcine hearts were obtained from a local abattoir. The left and noncoronary cusps of each aortic valve were excised. Cusps were submerged in room temperature (18 to 23 °C) coronary perfusion solution for a minimum of 100 min, a time sufficient to achieve osmotic equilibrium (Talman and Boughner 2001), before imaging in the same fluid. Specimens were secured to a rubber mat with the ventricularis facing upward by stretching elastic bands across their periphery. Care was taken to ensure the specimens were not visibly compressed by the elastic bands.

Data acquisition

Ultrasound imaging was performed using a Vevo 770 high-frequency micro-imaging system (VisualSonics Inc., Toronto, ON, Canada) equipped with a mechanically scanned, single-element transducer (model RMV-704) with an *f*-number of 2.0 and a nominal center frequency of 40 MHz. The transducer possessed an axial–lateral spatial resolution of approximately 40×80 μm^2, a 2-mm depth-of-field, and a 6-mm focal distance. Images were acquired with the tissue centered at the focus such that the bulk of the specimen was contained within the depth-of-field.

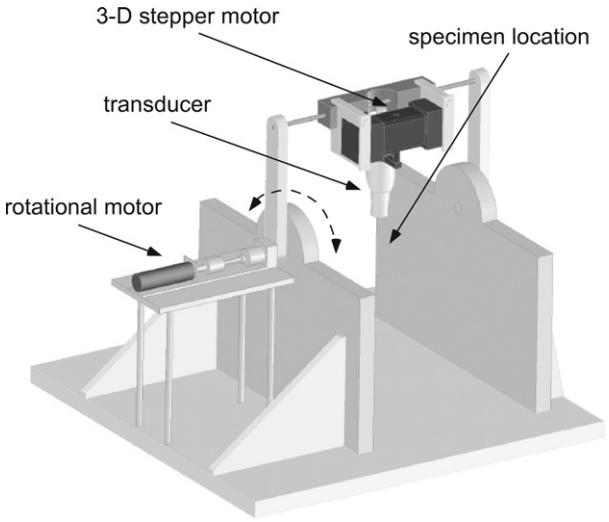

Fig. 2. Computer-assisted design drawing of the transducer angular positioning device used to control the angle of insonification for integrated backscatter measurements.

The radiofrequency (RF) echo signals needed for integrated backscatter analysis, as well as line and frame trigger signals, were accessible from BNC terminals on the scanner. The RF signals were sampled at 1 GHz and digitized into 8-bit data using an oscilloscope (Waverunner LT345, Lecroy Corp., Chestnut Ridge, NY, USA) and software written in LabVIEW 6.1 (National Instruments Corp., Austin, TX, USA). For each backscatter measurement, the software acquired RF signals corresponding to all 377 scan lines in the $8 \times 8\text{-mm}^2$ B-mode field-of-view.

For each cusp, backscatter measurements were acquired along two vertical planes of rotation to characterize biaxial anisotropy in the tissue. The first rotational plane was aligned with the circumferential axis of the cusp, and the second plane was approximately normal to the first, *i.e.,* along the radial axis of the cusp. A transducer angular positioning device, illustrated in Fig. 2, was built to rotate the transducer about its focus in a single plane. The rotational servomotor of the positioning device was driven by a PID servo driver (Motion Controller Module MVP2001B02, MicroMo, Clearwater, FL, USA) that rotated the transducer with a calculated precision of 0.0011°. The B-mode image sector,

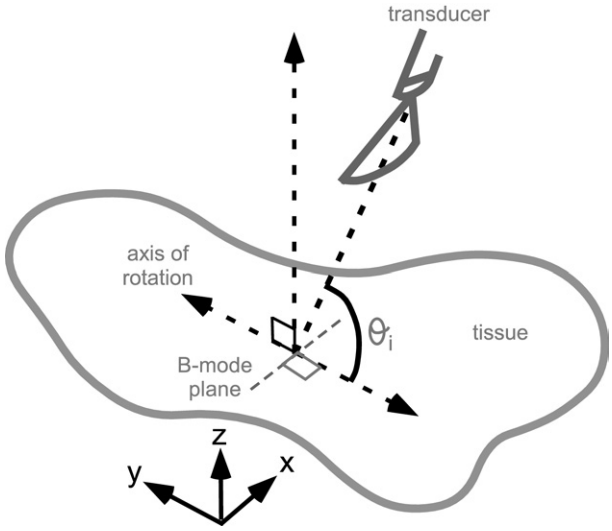

Fig. 3. Geometry of rotation of the ultrasound imaging plane during integrated backscatter measurements. The angle of insonification is denoted by θ_i.

which subtended an azimuth angle of approximately 7.5°, was always perpendicular to the plane of rotation as shown in Fig. 3, such that each scan line intersected the specimen at approximately the same angle and the tissue was positioned at the same depth throughout the field-of-view. Measurements were acquired from near the center of the cusp at angles of insonification (θ_i in Fig. 3) ranging from 50–130° in 10° increments, where $\theta_i = 90°$ corresponds to insonification in a vertical plane perpendicular to the specimen surface.

Ten RF frames were acquired at each insonification angle and averaged to reduce electronic noise. Complete data acquisition for a single specimen lasted approximately 100 min. Specimens were inspected throughout the procedure to ensure that no visible degradation of the tissue occurred.

Integrated backscatter processing

Processing of RF data was performed offline using MATLAB 7.1 (The MathWorks Inc., Natick, MA, USA). Because the transducer's nominal lateral beamwidth was 80 μm, every fourth scan line, separated by approximately 85 μm, was included in analysis. Therefore, a maximum of 95 independent RF signals, subject to the minimum-gate-length constraint described in the following paragraph, were analyzed at each insonification angle.

Hamming-window range gates were defined for each RF signal by selecting a two-dimensional region-of-interest in the corresponding B-mode image. The region was defined to include as much of the scattered signal from the interior of the specimen as possible while excluding the specular reflections from the surfaces. Therefore, the length of the range gate varied with the thickness of the specimen. Range gates were centered near the focus and always kept within the depth-of-field. Gates shorter than four pulse lengths, approximately 180 ns, in duration were excluded from the analysis as recommended by Lizzi et al. (1983). Gates greater than 1.33 μs in duration, the time for the pulse to traverse the depth-of-field, were truncated equally at both ends to exclude echoes from outside the depth-of-field.

Apparent integrated backscatter (AIB) was computed by normalizing the power spectrum of the windowed tissue signal by the power spectrum of a Hamming-windowed echo from a reference reflector and then integrating over the measured −6 dB bandwidth of the system. The reference reflector was a polished quartz flat (part 43424, Edmund Industrial Optics Inc., Barrington, NJ, USA) placed normal to the beam at the focus. To avoid saturating the oscilloscope, the transmit power and receive gain were decreased by 30 and 20 dB, respectively, for acquisition of the reference signal. Separate measurements using a tissue-mimicking phantom confirmed that the overall frequency response of the ultrasound system was consistent at the two gain settings (unpublished data). Therefore, at each insonification angle, the average tissue power spectrum was computed as

$$\left|V(f)\right|^2 = \frac{1}{N}\sum_{n=1}^{N}\frac{1}{L_n}\left|V_n(f)\right|^2, \quad (1)$$

where $V_n(f)$ is the Fourier transform of the RF signal corresponding to the nth scan line, L_n is the length of the range gate applied to the nth scan line and $N \approx 95$ is the number of independent scan lines. Apparent integrated backscatter (AIB) was then calculated as

$$AIB = 10\log_{10}\left(\int_{f_0-\frac{\Delta f}{2}}^{f_0+\frac{\Delta f}{2}}\frac{\left|V(f)\right|^2}{\frac{1}{L_{ref}}\left|V_{ref}(f)\right|^2}df\right) - G, \quad (2)$$

where f_0 is the center frequency and Δf is the −6 dB bandwidth of the system, $V_{ref}(f)$ is the Fourier transform of the reference signal, L_{ref} is the length of the window applied to the reference signal and $G = 50$ dB is the difference in gain settings during acquisition of the tissue and reference signals. The resulting quantity is properly referred to as the *apparent* integrated backscatter because no corrections were made for attenuation or diffraction (Hoffmeister et al. 1995).

Angular dependence of AIB was characterized using the method of Mottley and Miller (1988). AIB was plotted as a function of insonification angle, and the function

$$AIB(\theta_i) = A + B\cos\left[\frac{2\pi}{180^\circ}(\theta_i - \phi)\right], \qquad (3)$$

where θ_i and ϕ are both specified in degrees, was fit to the data using the nonlinear least-squares curve-fitting function in the MATLAB Optimization Toolbox. For each specimen and each direction of rotation, the curve-fitting procedure yielded values for the mean AIB, *A,* the amplitude of angular variation in AIB, *B,* and the insonification angle that produced the maximum AIB, ϕ. The coefficient of determination, R^2, was computed for each fitted curve as a measure of goodness of fit.

Statistical analysis

The mean values of *A, B* and R^2 obtained from rotation about the eight specimens in the circumferential and radial directions were compared using paired two-tailed *t*-tests. The mean values of ϕ obtained for each direction of rotation were compared with 90°, the expected value for rotation about the long axes of aligned cylindrical scatterers, using one-sample, two-tailed *t*-tests.

RESULTS

Representative RF signals from the reference reflector and a porcine aortic valve cusp are shown in Figs. 4a and b, respectively. Figure 4c shows the power spectrum of the reference signal, the average tissue power spectrum computed by applying eqn (1) to the ensemble of RF scan lines acquired from the specimen depicted in Fig. 4b and the result of normalizing that average tissue

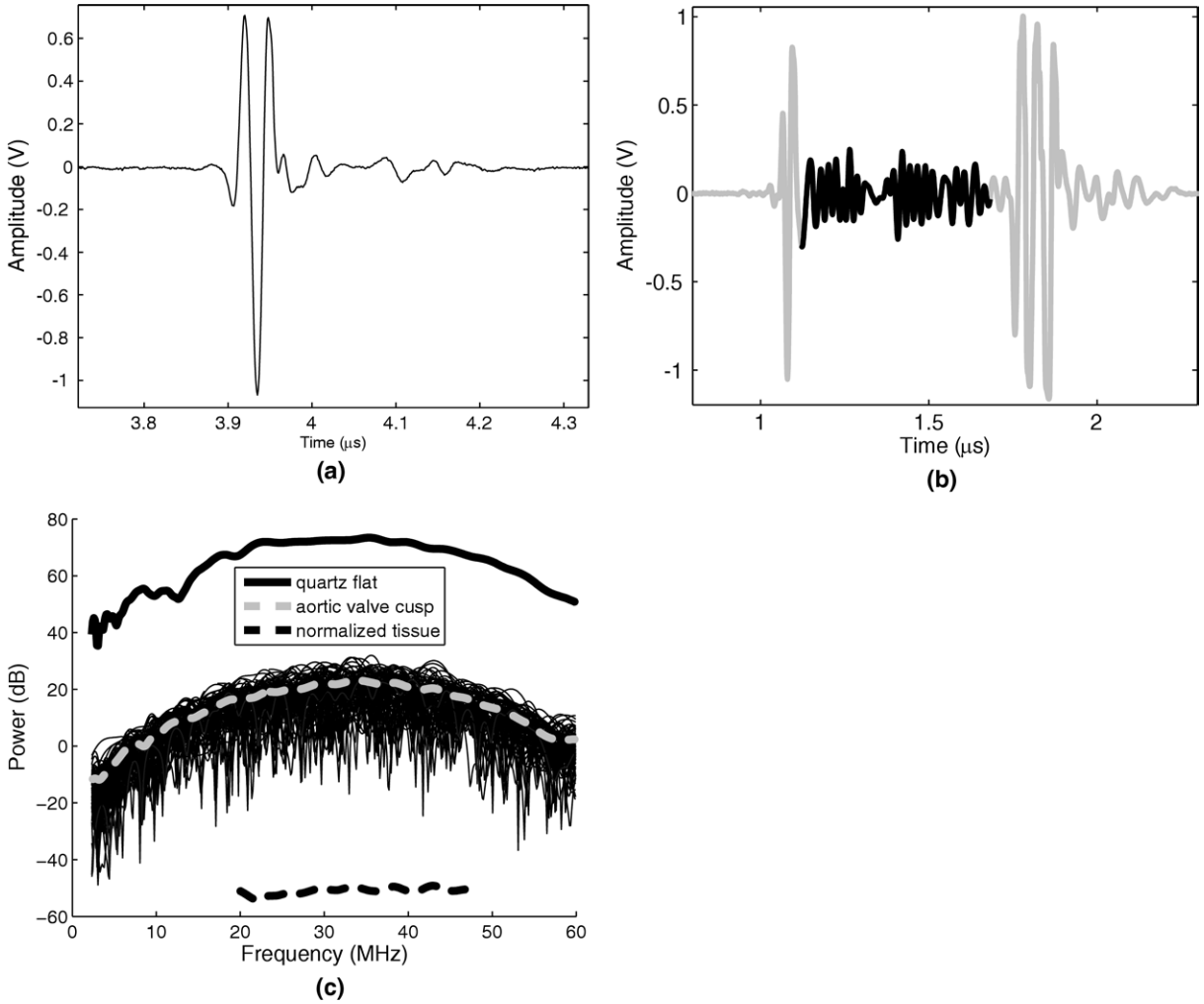

Fig. 4. (a) Radiofrequency echo signal obtained from the reference reflector. (b) Representative RF echo signal from a porcine aortic valve cusp, which was acquired using 50 dB greater system gain than the reference signal. The bold portion of the signal corresponds to the location of the user-selected range gate. (c) Power spectrum of echoes from the reference reflector (black, solid curve), mean power spectrum of echoes from an aortic valve cusp (grey, dashed curve) and the result of normalizing the mean tissue spectrum by the reference spectrum (black dashed curve). The thin, black, solid curves depict the power spectra of each scan line acquired from the tissue specimen.

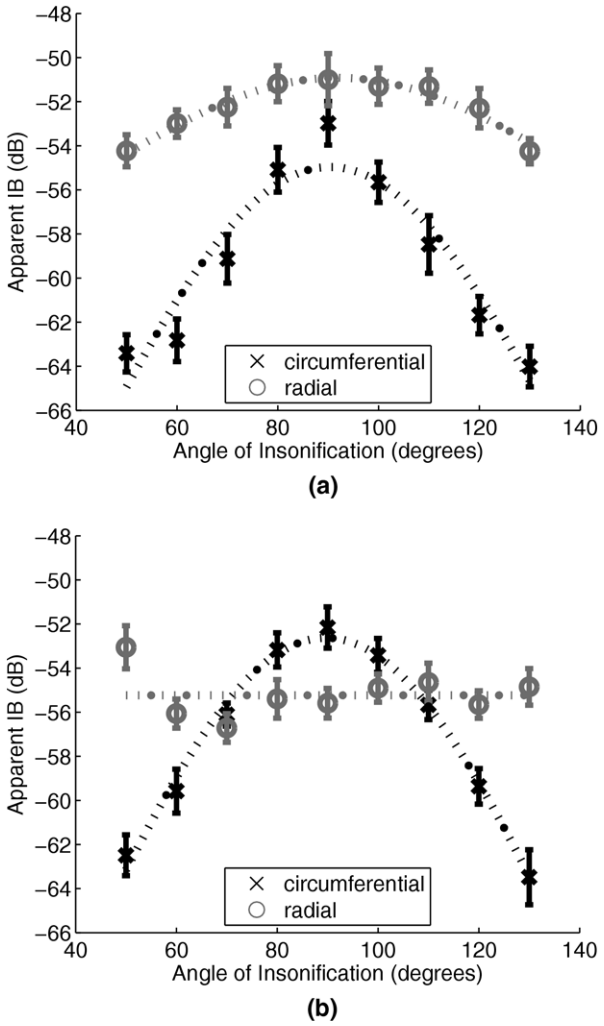

Fig. 5. (a) Apparent integrated backscatter as a function of angle of insonification for the aortic valve cusp that exhibited the greatest angular variation of backscatter in the radial direction. Data obtained during rotation in the circumferential direction (black crosses) and radial direction (grey circles) are plotted separately. The dashed curves represent sinusoidal functions fit to the data using eqn (3). (b) Angular dependence of apparent integrated backscatter for the cusp that exhibited the least variation in the radial direction. Each data point in both panels represents the mean AIB from many scan lines and the error bars indicate ±1 standard deviation from the mean.

spectrum by the reference spectrum. The reference spectrum indicates that the center frequency of the system was 33.6 MHz and the −6 dB bandwidth was 26.9 MHz.

Plots of AIB as a function of insonification angle are shown in Fig. 5 for the specimens that demonstrated the greatest and least angular dependence of backscatter in the radial direction. The curve-fitting results obtained for all eight specimens are summarized in Table 1 The mean amplitude of angular variation in AIB, *B,* was significantly greater in the circumferential direction than the radial direction, and the sinusoidal function of eqn (3) fit the circumferential data more consistently, as indicated by the significantly higher mean R^2 obtained for the circumferential data. The mean value of ϕ did not significantly differ from 90° in either the circumferential or the radial data.

Figure 6 shows the results of averaging the AIB data obtained from the eight cusps, plotting the averaged values as functions of insonification angle, and applying the curve-fitting procedure to the averaged data. Equation (3) describes the average angular variation in AIB well (*i.e.,* R^2 is close to 1.0) in both directions: the curve-fitting procedure yielded values of $B = 12.0$ dB, $\phi = 90.5°$ and $R^2 = 0.971$ in the circumferential direction and $B = 3.2$ dB, $\phi = 92.5°$ and $R^2 = 0.987$ in the radial direction. The amplitudes of angular variation in backscatter were greater in both directions of rotation than the average standard deviation of AIB over all cusps and all insonification angles, which was 2.2 dB and is indicative of the biological variability of the measurement.

DISCUSSION

From the perspective of the proposed application of integrated backscatter to nondestructive evaluation of tissue-engineered valves, the most encouraging result of this study is that anisotropy of high-frequency AIB can be detected in individual specimens, even when measurements are performed over a limited range of insonification angles. This assertion is best supported by the circumferential data, in which the lowest values of amplitude and R^2 for the fitted sinusoid were 7.35 dB and 0.893, respectively. However, the specimen-to-specimen variation in the ability of the sinusoidal function of eqn (3) to describe the radial angular dependence of backscatter was much greater: the fitted amplitude values range from 8.33 dB in Fig. 5a to 0 dB in Fig. 5b, and the radial R^2 values ranged from 0.959 to 0.209. The microstructural basis for this variability in the radial behavior of AIB from natural cusps should be clarified before the technique is applied to assess tissue-engineered valves.

The consistently high circumferential angular variation in AIB, combined with the fact that collagen fibers in the fibrosa tend to align in the circumferential direction, suggests that collagen is the primary source of scattering from aortic valve cusps. The AIB measurements were only acquired near the center of the cusps, but the preferred circumferential alignment of collagen is believed to prevail throughout the fibrosa (Sacks et al. 1998). The stiffness and abundance of the collagen fiber bundles, as well as the evidence implicating collagen as the primary scattering source from other cardiac tissues (Mimbs et al. 1980; O'Donnell et al. 1981; Lythall et al. 1993; Chandraratna et al. 1997), provides additional sup-

Table 1. Parameters of sinusoidal functions fit to angular variation of AIB from porcine aortic valve cusps

Axis	A (dB)	B (dB)	ϕ (°)	R^2
Circumferential	–64.8 ± 2.7*	12.1 ± 2.6*	90.5 ± 2.7†	0.94 ± 0.04‡
Radial	–56.8 ± 2.5	3.5 ± 3.1	94.7 ± 12.3†	0.66 ± 0.30

A = Mean AIB; B = amplitude of angular variation; ϕ = angle of maximum AIB, as defined in eqn. (3).
Data are mean ± standard deviation for eight specimens.
* $p = 0.002$ *vs.* radial.
† $p > 0.3$ *vs.* 90°.
‡ $p = 0.048$ *vs.* radial.

port to this hypothesis. On the other hand, Hall et al. (2000) demonstrated that, in canine aortic arterial tissue at 30–45 MHz, ultrasonic backscatter is dominated by the elastin content of the tissue, despite the abundance of collagen. However, the weaker anisotropy of backscatter in the radial direction of the cusps, along which elastin fibers in the ventricularis tend to align (Vesely and Noseworthy 1992), suggests that scattering from elastin is less prominent than scattering from collagen in aortic valve cusps.

The range gates applied during the AIB analysis encompassed echoes from all three tissue layers, so it was reasonable to expect angular dependence of backscattering to be evident in both the circumferential and radial directions. This approach was used because the objective of this study was simply to determine the magnitude of angular variation in AIB that can be expected from aortic valve cusps at high frequencies. The proposed application to tissue-engineered valves will require the capability to characterize anisotropy of backscatter from the fibrosa and ventricularis individually so AIB measurements can be used to confirm that an engineered valve adequately mimics the structure of a natural valve. It should be possible to define range gates to select individual layers of a cusp by segmenting B-mode images, as demonstrated by Qiu et al. (2006). The 180-ns minimum gate length, which corresponds to a minimum layer thickness of about 140 μm, poses one possible constraint on this type of measurement, because the layer thicknesses in a natural cusp vary with position and, in porcine specimens at least, can be <140 μm at some locations (Khan et al. 2007). However, it may be sufficient to confirm proper fiber alignment at a few locations rather than attempting to map fiber orientation throughout the specimen volume, such that AIB measurements could be performed selectively where the tissue layers are thickest.

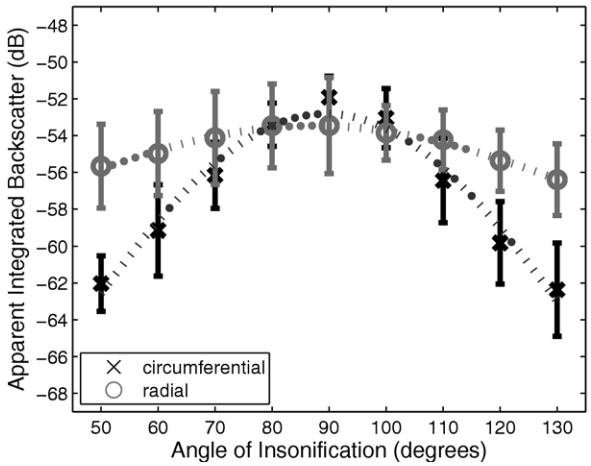

Fig. 6. Ensemble mean AIB from eight porcine aortic valve cusps as a function of angle of insonification. Data obtained during rotation in the circumferential direction (black crosses) and radial direction (grey circles) are plotted separately. The dashed curves represent sinusoidal functions fit to the data using eqn. (3). Error bars indicate ±1 standard deviation from the mean.

The calculation of AIB does not include compensation for attenuation or diffraction. Attenuation can exhibit an angular dependence in the presence of aligned microstructure (Baldwin et al. 2006), which can influence the angular dependence of AIB. In this study, the amount of intervening tissue, and therefore attenuation, was minimal because thin tissue specimens were imaged *in vitro*. When using a high-frequency, highly-focused transducer, such as the *f*-number 2.0 aperture in this study, diffraction can also cause substantial depth-dependent changes in backscatter intensity (Machado and Foster 1999). However, the same instrument was used for all measurements and the regions-of-interest for AIB analysis were confined to the focal zone of the transducer, so any diffraction effects should be similar in each specimen. Therefore, neither attenuation nor diffraction should have influenced the conclusions drawn from the AIB data.

The use of a variable range–gate length is less than ideal, but is a constraint imposed by the morphology of the specimens. When backscatter is measured from thick slabs of tissue, it is advisable to use a consistent window with length substantially greater than the four-pulse-length minimum on all scan lines to reduce the variance

of the AIB estimates and ensure that the contributions of attenuation and diffraction are uniform in each scan line. However, in the experiments reported here, it was necessary to exclude the specular reflections from external surfaces that are illustrated in Fig. 4b. One approach that was considered and rejected would have involved specifying a relatively long, fixed gate length and ignoring all scan lines where the tissue was thinner than the gate, but this approach would have yielded a low, and highly variable, number of usable scan lines for many insonification angles. A variable gate length was thus a compromise between these competing factors.

Although the 100-min duration of data acquisition was relatively long, the properties of the specimens should remain stable during this period. First, recall that the specimens were soaked in coronary perfusion solution for an additional 100 min to ensure that they had reached osmotic equilibrium before the beginning of data acquisition. Second, Lovekamp et al. (2006) demonstrated that the extracellular matrix of cusp specimens was not altered by submersion in saline for up to five hours, and coronary perfusion solution provides a more physiologic environment for the specimens than simple saline. The data support this assumption, because the $\theta_i = 90°$ measurements taken 50 min apart during rotation in the circumferential and radial directions were consistent with one another and because the measured AIB was symmetric about $\theta_i = 90°$ despite the fact that the extreme measurements (*i.e.,* $\theta_i = 50°$ and $\theta_i = 130°$) were also typically acquired 50 min apart.

Optical techniques, specifically confocal microscopy and optical coherence tomography (OCT), are the most developed methods for nondestructive evaluation of engineered tissues (Tan et al. 2004; Yang et al. 2006). Both methods produce 3-D images. Confocal microscopy provides resolution comparable to conventional histology, with penetration depths up to a few hundred microns. The performance of OCT is comparable to high-frequency ultrasound, with slightly finer resolution, on the order of 10 μm, and penetration depths of about 2–3 mm, which would be sufficient for imaging heart valve cusps. Fiber alignment can be detected with impressive precision using polarization-sensitive OCT (Ugryumova et al. 2006; Xie et al. 2006). As high-frequency ultrasound techniques are developed further, it will be necessary to compare them with optical methods with respect to their utility and efficiency for nondestructive evaluation of engineered tissues.

If, in addition to the tissue-engineering application, ultrasonic scattering is also to be used as a clinical measure of natural or implanted valve condition, it is clear from the results of this study that the anisotropy of scattering must be considered. For example, Rigolin et al. (2001) reported differences ranging from 1.7–3.5 dB in integrated backscatter amplitude at 2.5–7.0 MHz between unused and explanted porcine bioprosthetic aortic valve cusps *in vitro.* Our data, although acquired at higher frequencies, suggest that such differences could be caused by deviations of $<10°$ in insonification angle.

CONCLUSIONS

This study demonstrates that high-frequency AIB from *ex vivo* porcine aortic valve cusps exhibits substantial anisotropy that can be detected in measurements acquired over a limited range of insonification angles. The relative amplitudes of angular variation of AIB in the circumferential and radial directions imply that collagen fibers in the fibrosa are the principal source of high-frequency scattering from valve cusps, whereas smaller contributions are made by collagen or elastin fibers in the ventricularis. The ability to detect anisotropy of backscatter in individual specimens indicates that the technique can be applied to nondestructive evaluation of fiber alignment in tissue-engineered prosthetic valves.

Acknowledgments—We thank Joy Dunmore-Buyze for assistance with acquisition and preparation of the tissue specimens; Youcef Brahimi, Abdul Naeem and Adam Waspe for assistance with design and characterization of the transducer angular positioning device; Amanda Hamilton for assistance with the histological image; and Lauren Wirtzfeld for assistance with characterization of the ultrasound system gain. This research was funded by Heart and Stroke Foundation of Ontario Grant NA5843, the Ontario Research and Development Challenge Fund, and the University of Western Ontario Schulich School of Medicine and Dentistry. Zamir Khan was supported by an Ontario Graduate Scholarship and the Canadian Institutes of Health Research Strategic Training Program in Vascular Research.

REFERENCES

Baldwin SL, Marutyan KR, Yang M, Wallace KD, Holland MR, Miller JG. Measurements of the anisotropy of ultrasonic attenuation in freshly excised myocardium. J Acoust Soc Am 2006;119:3130–3139.

Bashey RI, Torii S, Angrist A. Age-related collagen and elastin content of human heart valves. J Gerontol 1967;22:203–208.

Chandraratna PAN, Whittaker P, Chandraratna PM, Gallet J, Kloner RA, Hla A. Characterization of collagen by high-frequency ultrasound: Evidence for different acoustic properties based on collagen fiber morphologic characteristics. Am Heart J 1997;133:364–368.

Christie GW. Computer modeling of bioprosthetic heart valves. Eur J Cardiothorac Surg 1992;6:S95–S100.

Christie GW, Barratt-Boyes BG. Biaxial mechanical properties of explanted aortic allograft leaflets. Ann Thorac Surg 1995;60:S160–S164.

Doehring TC, Kahelin M, Vesely I. Mesostructures of the aortic valve. J Heart Valve Dis 2005;14:679–686.

Hall CS, Nguyen CT, Scott MJ, Lanza GM, Wickline SA. Delineation of the extracellular determinants of ultrasonic scattering from elastic arteries. Ultrasound Med Biol 2000;26:613–620.

Hoffmeister BK, Wong AK, Verdonk ED, Wickline SA, Miller JG. Comparison of the anisotropy of apparent integrated ultrasonic backscatter from fixed human tendon and fixed human myocardium. J Acoust Soc Am 1995;97:1307–1313.

Insana MF. Modeling acoustic backscatter from kidney microstructure using an anisotropic correlation function. J Acoust Soc Am 1995;97:649–655.

Khan Z, Boughner DR, Lacefield JC. Reconsidering the layer thickness distribution in aortic valve cusps using high-frequency ultrasound. Proc Intl Symp Biomed Imaging 2007:868–871.

Lattanzi F, Picano E, Landini L, Mazzarisi A, Pelosi G, Benassi A, Salvatore L, Distante A, L'Abbate A. In vivo identification of mitral valve fibrosis and calcium by real-time quantitative ultrasonic analysis. Am J Cardiol 1990;65:355–359.

Lizzi FL, Greenebaum M, Feleppa EJ, Elbaum M, Coleman DJ. Theoretical framework for spectrum analysis in ultrasonic tissue characterization. J Acoust Soc Am 1983;73:1366–1373.

Lovekamp JJ, Simionescu DT, Mercuri JJ, Zubiate B, Sacks MS, Vyavahare NR. Stability and function of glycosaminoglycans in porcine bioprosthetic heart valves. Biomaterials 2006;27:1507–1518.

Lythall DA, Bishop J, Greenbaum RA, Ilsley CJD, Mitchell AG, Gibson DG, Yacoub MH. Relationship between myocardial collagen and echo amplitude in non-fibrotic hearts. Eur Heart J 1993; 14:344–350.

Machado JC, Foster FS. Validation of theoretical diffraction correction functions for strongly focused high frequency ultrasonic transducers. Ultrason Imaging 1999;21:96–106.

Mendelson K, Schoen FJ. Heart valve tissue engineering: Concepts, approaches, progress, and challenges. Ann Biomed Eng 2006;34: 1799–1819.

Mimbs JW, O'Donnell M, Bauwens D, Miller JW, Sobel BE. The dependence of ultrasonic attentuation and backscatter on collagen content in dog and rabbit hearts. Circ Res 1980;47:49–58.

Mottley JG, Miller JG. Anisotropy of the ultrasonic backscatter of myocardial tissue: I. Theory and measurements in vitro. J Acoust Soc Am 1988;83:755–761.

O'Donnell M, Mimbs JW, Miller JG. Relationship between collagen and ultrasonic backscatter in myocardial tissue. J Acoust Soc Am 1981;69:580–588.

Qiu Q, Dunmore-Buyze J, Boughner DR, Lacefield JC. Evaluation of an algorithm for semiautomated segmentation of thin tissue layers in high-frequency ultrasound images. IEEE Trans Ultrason Ferroelectr Freq Control 2006;53:324–334.

Rigolin VH, Vonesh MJ, Ng KH, Roth SI, Sehgal R, McPherson DD, Mehlman DJ. Structural evaluation of porcine heart valve bioprostheses with radiofrequency ultrasound. Cardiovasc Pathol 2001;10: 179–188.

Rose JH, Kaufmann MR, Wickline SA, Hall CS, Miller JG. A proposed microscopic elastic wave theory for ultrasonic backscatter from myocardial tissue. J Acoust Soc Am 1995;97:656–668.

Sacks MS, Smith DB, Hiester ED. The aortic valve microstructure: Effects of transvalvular pressure. J Biomed Mater Res 1998;41: 131–141.

Shi V, Rittman L, Vesely I. Novel geometries for tissue engineered tendonous constructs. Tissue Eng 2006;12:2601–2609.

Talman EA, Boughner DR. Effect of altered hydration on the internal shear properties of porcine aortic valve cusps. Ann Thorac Surg 2001;71:S375–S378.

Tan W, Sendemir-Urkmez A, Fahrner LJ, Jamison R, Leckband D, Boppart SA. Structural and functional optical imaging of three-dimensional engineered tissue development. Tissue Eng 2004;10: 1747–1756.

Thubrikar M. The Aortic Valve. Boca Raton, FL: CRC Press, 1995: 221.

Ugryumova N, Gangnus SV, Matcher SJ. Three-dimensional optic axis determination using variable-incidence-angle polarization-optical coherence tomography. Opt Lett 2006;31:2305–2307.

Vesely I. The evolution of bioprosthetic heart valve design and its impact on durability. Cardiovasc Pathol 2003;12:277–286.

Vesely I, Boughner D. Analysis of the bending behavior of porcine xenograft leaflets and of neutral aortic valve material: Bending stiffness, neutral axis, and shear measurements. J Biomech 1989; 22:655–671.

Vesely I, Noseworthy R. Micromechanics of the fibrosa and the ventricularis in aortic valve leaflets. J Biomech 1992;25:101–113.

Xie T, Guo S, Zhang J, Chen Z, Peavy GM. Use of polarization-sensitive optical coherence tomography to determine the directional polarization sensitivity of articular cartilage and meniscus. J Biomed Opt 2006;11:064001-1–064001-8.

Yang Y, Dubois A, Qin X-P, Li J, Haj AE, Wang RK. Investigation of optical coherence tomography as an imaging modality in tissue engineering. Phys Med Biol 2006;51:1649–1659.